Modal Expansion Analysis of T-Shaped Waveguide

HUAPENG ZHAO [ID], (Member, IEEE), KANGNING LI [ID], (Student Member, IEEE), AND MINGZHOU ZHAN, (Member, IEEE)

School of Electronic Science and Engineering, University of Electronic Science and Technology, Chengdu 611731, China

Corresponding author: Huapeng Zhao (huapengzhao@uestc.edu.cn)

ABSTRACT The T-shaped waveguide (T-waveguide for short) is a new kind of wideband waveguide which is easier to fabricate than conventional wideband waveguides. This paper presents the modal expansion analysis of the T-waveguide. The T-waveguide is first divided into four rectangular domains. The electromagnetic fields in each domain are expressed by suitable mode functions. The continuity of tangential electromagnetic fields along the interface of neighboring regions is enforced by the Galerkin's matching process and a matrix equation is thus derived. The cutoff wavenumbers of the T-waveguide are then found from the matrix. The results are in good agreement with those obtained by CST Microwave Studio. The proposed method provides fast calculation of the T-waveguide cutoff wavenumber, which is of guiding significance to the design of T-waveguide.

INDEX TERMS T-waveguide, modal expansion, boundary condition, Galerkin matching, cutoff wavenumber.

I. INTRODUCTION

Waveguide has been widely used because of the effectiveness and reliability in microwave power transmission [1]. Due to its features of low energy loss and high power capacity, it can be used for power dividers and directional couplers to improve power combining efficiency [2]–[5]. In [6]–[8], waveguide is used as filters for its advantage of wide bandwidth and simple structure. In [9] and [10], waveguide amplifier with high gain and miniaturization is introduced. In addition, waveguide slot antenna array has attracted much attention in recent years because of its compact structure, high radiation efficiency and good stability [11]–[14]. According to microwave theory [1], the performance of waveguide depends largely on the size and shape of the cross section, which determine the propagation characteristics of the waveguide. Generally, the microwave transmission system should work in the single mode transmission state [15], because single mode transmission is easy to excite and couple, and there is no energy conversion between modes, which avoids the signal distortion caused by the transmission of different modes at different speeds. The simplest method of realizing single mode transmission is to select the lowest mode as the operation mode, while keeping all higher

modes in the cut-off state. Rectangular waveguide [1], as a common microwave device, is simple in structure but limited by its single mode bandwidth. Double ridged waveguide has a broadband characteristic, but the structure is inconvenient to fabricate. The T-waveguide has wide single mode bandwidth and simple structure, but its fast analysis has not been investigated.

In the past few years, many methods have been proposed for the analysis of waveguides. In [16], a cubic-order subparametric finite element technique is utilized to compute the eigenvalues of arbitrarily shaped waveguide structure. In [17], the authors used a high order symplectic compact finite-difference time-domain algorithm to analyze the dispersion and resonant frequency of the waveguide. The modal-expansion method, due to its good accuracy and effectiveness, is commonly used to analyze waveguides [18]–[20] and antennas [21], [22]. Based on modal expansion method, this paper introduces a realistic and rigorous analysis for the T-waveguide. For the whole T-waveguide structure, it can be decomposed into four simple regions. And in each region, the modal equations satisfying the Maxwell equation can be found. Each region can be expanded with a series of known pattern functions, and the boundary conditions can be applied to solve the expansion coefficients. Then, the Galerkin matching is used to impose boundary conditions on the interfaces of these regions. Combining these

---

The associate editor coordinating the review of this manuscript and approving it for publication was Wu-Shiung Feng.
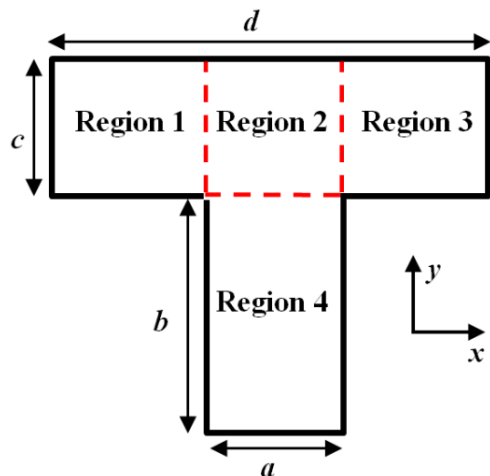
FIGURE 1. Illustration of a T-shaped waveguide.

two processes, a set of matrix equations can be derived with regard to the unknown field expansion coefficients. From the matrix, the cutoff wavenumber or single mode bandwidth of T-waveguide can be obtained. It should be mentioned that the modal expansion method has been used to analyze a ridge waveguide whose mode symmetric plane is a magnetic wall [23]. The T-waveguide is equivalent to a ridge waveguide whose mode symmetric plane is an electric wall, which makes the boundary conditions and mode functions in this work different from the analysis of ridge waveguide.

The rest of this paper is organized as follows. In Section II, formulations of field expansion and matching process are presented. Section III presents the verification of the proposed method. Section IV concludes this work.

II. FORMULATIONS OF THE METHOD

A. REGION DIVISION

The geometry of the T-waveguide is shown in Fig. 1 along with the dimensional notations. The T-waveguide is decomposed into four regions. For every region, a local rectangular coordinate system can be constructed. Assume the origin of the local coordinate system is chosen as the bottom-left point of the region. Consider the waveguide working in TE mode. Using the following relationship between longitudinal magnetic field and transverse electric fields,

$$E_x = \frac{-j\omega\mu}{k_c^2}\frac{\partial H_z}{\partial y}, \quad E_y = \frac{j\omega\mu}{k_c^2}\frac{\partial H_z}{\partial x}, \quad (1)$$

and based on the boundary conditions of every region, the expression of the transverse electric fields for every region can be derived.

B. FIELD EXPANSION

In a rectangular domain, the general expression of the longitudinal magnetic field satisfying the TE wave

equation is

$$
\begin{aligned}
H_z(x, y) &= \sum_{n=0}^{N} (A_n \cos(k_{xn}x) + B_n \cos[k_{xn}(D_x - x)]) \cos\frac{n\pi y}{D_y} \\
&+ \sum_{m=0}^{M} \left(C_m \cos(k_{ym}y) + D_m \cos[k_{ym}(D_y - y)]\right) \cos\frac{m\pi x}{D_x}
\end{aligned}
\tag{2}
$$

where A_n, B_n, C_m and D_m are the unknown field expansion coefficients. D_x and D_y are the dimensions of the rectangular domain along x- and y-directions, respectively, and

$$k_{xn} = \sqrt{k_c^2 - (n\pi/D_y)^2}, \quad k_{ym} = \sqrt{k_c^2 - (m\pi/D_x)^2}.$$

In Region 1, based on the boundary conditions $E_y|_{x=0} = 0$, $E_x|_{y=0} = 0$, and $E_x|_{y=c} = 0$. From (1) and (2), the electromagnetic fields can be expressed as

$$H_z^I(x, y) = \sum_{n=0}^{N} A_n^I \cos(k_{xn}x) \cos\frac{n\pi y}{c} \tag{3}$$

$$E_x^I(x, y) = \frac{j\omega\mu}{k_c^2} \sum_{n=0}^{N} \frac{n\pi}{c} A_n^I \cos(k_{xn}x) \sin\frac{n\pi y}{c} \tag{4}$$

$$E_y^I(x, y) = \frac{-j\omega\mu}{k_c^2} \sum_{n=0}^{N} k_{xn} A_n^I \sin(k_{xn}x) \cos\frac{n\pi y}{c} \tag{5}$$

The boundary condition in Region 2 is $E_x|_{y=c} = 0$, and the electromagnetic fields in Region 2 are written as

$$
\begin{aligned}
H_z^{II}(x, y) &= \sum_{n=0}^{N} \left(A_n^{II}\cos(k_{xn}x) + B_n^{II}\cos[k_{xn}(a-x)]\right) \\
&\cdot \cos\frac{n\pi y}{c} + \sum_{m=0}^{M} D_m^{II}\cos[k_{ym}(c-y)]\cos\frac{m\pi x}{a}
\end{aligned}
\tag{6}
$$

$$
\begin{aligned}
E_x^{II}(x, y) &= \frac{j\omega\mu}{k_c^2}\left\{\sum_{n=0}^{N}\frac{n\pi}{c}\left\{A_n^{II}\cos(k_{xn}x) + B_n^{II}\cos[k_{xn}(a-x)]\right\}\right. \\
&\left.\cdot \sin\frac{n\pi y}{c} + \sum_{m=0}^{M}k_{ym}\left\{-D_m^{II}\sin[k_{ym}(c-y)]\right\}\cos\frac{m\pi x}{a}\right\}
\end{aligned}
\tag{7}
$$

$$
\begin{aligned}
E_y^{II}(x, y) &= \frac{-j\omega\mu}{k_c^2}\left\{\sum_{n=0}^{N}k_{xn}\left\{A_n^{II}\sin(k_{xn}x) - B_n^{II}\sin[k_{xn}(a-x)]\right\}\right. \\
&\left.\cdot \sin\frac{n\pi y}{c} + \sum_{m=0}^{M}\frac{m\pi}{a}\left\{D_m^{II}\cos[k_{ym}(c-y)]\right\}\sin\frac{m\pi x}{a}\right\}
\end{aligned}
\tag{8}
$$

In Region 3, the boundary conditions are $E_y|_{x=(d-a)/2} = 0$, $E_x|_{y=0} = 0$, and $E_x|_{y=c} = 0$. From (1) and (2), the

electromagnetic fields in Region 3 are

$$H_z^{III}(x, y) = \sum_{n=0}^{N} B_n^{III} \cos[k_{xn}((d-a)/2 - x)] \cos \frac{n\pi y}{c} \quad (9)$$

$$E_x^{III}(x, y) = \frac{j\omega\mu}{k_c^2} \left\{ \sum_{n=0}^{N} \left\{ B_n^{III} \cos[k_{xn}((d-a)/2 - x)] \right\} \right.$$
$$\left. \cdot \frac{n\pi}{c} \sin \frac{n\pi y}{c} \right\} \quad (10)$$

$$E_y^{III}(x, y) = \frac{j\omega\mu}{k_c^2} \left\{ \sum_{n=0}^{N} \left\{ B_n^{III} \sin[k_{xn}((d-a)/2 - x)] \right\} \right.$$
$$\left. \cdot k_{xn} \cos \frac{n\pi y}{c} \right\} \quad (11)$$

Similarly, the electromagnetic fields in Region 4 are

$$H_z^{IV}(x, y) = \sum_{m=0}^{M} C_m^{IV} \cos(k_{ym}y) \cos \frac{m\pi x}{a} \quad (12)$$

$$E_x^{IV}(x, y) = \frac{j\omega\mu}{k_c^2} \left\{ \sum_{m=0}^{M} k_{ym} \left\{ C_m^{IV} \sin(k_{ym}y) \right\} \cos \frac{m\pi x}{a} \right\} \quad (13)$$

$$E_y^{IV}(x, y) = \frac{-j\omega\mu}{k_c^2} \left\{ \sum_{m=0}^{M} \frac{m\pi}{a} \left\{ C_m^{IV} \cos(k_{ym}y) \right\} \sin \frac{m\pi x}{a} \right\} \quad (14)$$

C. MATCHING PROCESS
The continuity boundary conditions across the interface of the Regions 1 and 2 are

$$H_z^I(x = (d-a)/2, y) = H_z^{II}(x = 0, y) \quad y \in (0, c) \quad (15)$$
$$E_y^I(x = (d-a)/2, y) = E_y^{II}(x = 0, y) \quad y \in (0, c) \quad (16)$$

Substituting equations (3) and (6) into equation (15), and equations (5) and (8) into (16), one can have

$$\sum_{n=0}^{N} k_{xn} A_n^I \sin(k_{xn}(d-a)/2) \cos \frac{n\pi y}{c}$$
$$= \sum_{n=0}^{N} k_{xn} \left[-B_n^{II} \sin(k_{xn}a) \right] \cos \frac{n\pi y}{c} \quad (17)$$

$$\sum_{n=0}^{N} A_n^I \cos(k_{xn}(d-a)/2) \cos \frac{n\pi y}{c}$$
$$= \sum_{n=0}^{N} \left(A_n^{II} + B_n^{II} \cos(k_{xn}a) \right)$$
$$\cdot \cos \frac{n\pi y}{c} + \sum_{m=0}^{M} D_m^{II} \cos[k_{ym}(c - y)] \quad (18)$$

By taking the inner products of the equations (17) and (18) with $\cos \frac{q\pi y}{c}$ and $\cos \frac{p\pi y}{c}$, respectively, $(q = 0, 1, 2, \cdots, Y_{12}$

and $p = 0, 1, 2, \cdots, Y_{12}$, where Y_{12} is equal to the smaller one of N and M), the following matrix equations are obtained

$$\mathbf{L_1 a^I} = \mathbf{L_2 a^{II}} + \mathbf{L_3 b^{II}} + \mathbf{L_4 d^{II}} \quad (19)$$
$$\mathbf{K_1 a^I} = \mathbf{K_2 b^{II}} \quad (20)$$

where $\mathbf{a^I}$, $\mathbf{a^{II}}$, $\mathbf{b^{II}}$, $\mathbf{d^{II}}$ are vectors consisting of A_n^I, A_n^{II}, B_n^{II} and D_m^{II}, respectively, and the elements of matrices $\mathbf{L_1}$, $\mathbf{L_2}$, $\mathbf{L_3}$, $\mathbf{L_4}$, $\mathbf{K_1}$ and $\mathbf{K_2}$ are defined as follows

$$L_{1pn} = \int_0^c \cos \frac{p\pi y}{c} \cdot \cos(k_{xn} \frac{d-a}{2}) \cos \frac{n\pi y}{c} dy \quad (21)$$

$$L_{2pn} = \int_0^c \cos \frac{p\pi y}{c} \cdot \cos \frac{n\pi y}{c} dy \quad (22)$$

$$L_{3pn} = \int_0^c \cos \frac{p\pi y}{c} \cdot \cos(k_{xn}a) \cos \frac{n\pi y}{c} dy \quad (23)$$

$$L_{4pm} = \int_0^c \cos \frac{p\pi y}{c} \cdot \cos[k_{ym}(c - y)] dy \quad (24)$$

$$K_{1qn} = \int_0^c \cos \frac{q\pi y}{c} \cdot k_{xn} \sin(k_{xn} \frac{d-a}{2}) \cos \frac{n\pi y}{c} dy \quad (25)$$

$$K_{2qn} = \int_0^c -\cos \frac{q\pi y}{c} \cdot k_{xn} \sin(k_{xn}a) \cos \frac{n\pi y}{c} dy \quad (26)$$

The continuity boundary conditions across the interface of the Regions 2 and 3 are

$$H_z^{II}(x = a, y) = H_z^{III}(x = 0, y) \quad y \in (0, c) \quad (27)$$
$$E_y^{II}(x = a, y) = E_y^{III}(x = 0, y) \quad y \in (0, c) \quad (28)$$

Substituting equations (6) and (9) into (27), and equations (8) and (11) into (28), and invoking Galerkin's matching process, one can derive the following matrix equations

$$\mathbf{J_1 b^{III}} = \mathbf{J_2 a^{II}} + \mathbf{J_3 b^{II}} + \mathbf{J_4 d^{II}} \quad (29)$$
$$\mathbf{H_1 b^{III}} = \mathbf{H_2 a^{II}} \quad (30)$$

where $\mathbf{b^{III}}$ is a vector consisting of B_n^{III}, and the elements of matrices $\mathbf{J_1}$, $\mathbf{J_2}$, $\mathbf{J_3}$, $\mathbf{J_4}$, $\mathbf{H_1}$ and $\mathbf{H_2}$ are defined as follows

$$J_{1rn} = \int_0^c \cos \frac{r\pi y}{c} \cos \left(k_{xn} \frac{d-a}{2} \right) \cos \frac{n\pi y}{c} dy \quad (31)$$

$$J_{2rn} = \int_0^c \cos \frac{r\pi y}{c} \cos(k_{xn}a) \cos \frac{n\pi y}{c} dy \quad (32)$$

$$J_{3rn} = \int_0^c \cos \frac{r\pi y}{c} \cos \frac{n\pi y}{c} dy \quad (33)$$

$$J_{4rm} = \int_0^c \cos \frac{r\pi y}{c} \cos[k_{ym}(c - y)] \cos m\pi dy \quad (34)$$

$$H_{1sn} = \int_0^c -\cos \frac{s\pi y}{c} k_{xn} \sin[k_{xn}((d-a)/2)] \cos \frac{n\pi y}{c} dy \quad (35)$$

$$H_{2sn} = \int_0^c \cos \frac{s\pi y}{c} k_{xn} \sin(k_{xn}a) \cos \frac{n\pi y}{c} dy \quad (36)$$

where $r = 0, 1, 2, \cdots, Y_{23}$ and $s = 0, 1, 2, \cdots, Y_{23}$, where Y_{23} is equal to the smaller one of N and M.

The continuity boundary conditions across the interface of the Regions 2 and 4 are

$$E_x^{II}(x, y = 0) = E_x^{IV}(x, y = b) \quad (37)$$
$$E_y^{II}(x, y = 0) = E_y^{IV}(x, y = b) \quad (38)$$

Substituting equations (7) and (13) into (37), and equations (8) and (14) into (38), and applying Galerkin's matching process, one can derive the following matrix equations

$$\mathbf{U_1 d^{II} = U_2 c^{IV}} \tag{39}$$

$$\mathbf{O_1 c^{IV} = O_2 a^{II} + O_3 b^{II} + O_4 d^{II}} \tag{40}$$

where $\mathbf{c^{II}}$ is a vector constituted by C_m^{II}, and the elements of matrices $\mathbf{O_1}$, $\mathbf{O_2}$, $\mathbf{O_3}$, $\mathbf{O_4}$, $\mathbf{U_1}$ and $\mathbf{U_2}$ are defined as follows

$$U_{1tm} = \int_0^a -\cos\frac{t\pi x}{a} k_{ym} \sin\left(k_{ym}c\right) \cos\frac{m\pi x}{a} dx \tag{41}$$

$$U_{2tm} = \int_0^a \cos\frac{t\pi x}{a} k_{ym} \sin(k_{ym}b) \cos\frac{m\pi x}{a} dx \tag{42}$$

$$O_{1um} = \int_0^a \cos\frac{u\pi x}{a} \cos(k_{ym}b) \cos\frac{m\pi x}{a} dx \tag{43}$$

$$O_{2un} = \int_0^a \cos\frac{u\pi x}{a} \cos\left(k_{xn}x\right) dx \tag{44}$$

$$O_{3un} = \int_0^a \cos\frac{u\pi x}{a} \cos[k_{xn}(a-x)]dx \tag{45}$$

$$O_{4um} = \int_0^a \cos\frac{u\pi x}{a} \cos(k_{ym}c) \cos\frac{m\pi x}{a} dx \tag{46}$$

where $t = 0, 1, 2, \cdots, Y_{24}$ and $u = 0, 1, 2, \cdots, Y_{24}$, where Y_{24} is equal to the smaller number of N and M

Combining equations (19), (20), (29), (30), (39) and (40), the following matrix equation is obtained

$$\begin{bmatrix} \mathbf{L_2} & \mathbf{L_3 - L_1 K_1^{-1} K_2} & \mathbf{L_4} \\ \mathbf{J_2 - J_1 H_1^{-1} H_2} & \mathbf{J_3} & \mathbf{J_4} \\ \mathbf{O_2} & \mathbf{O_3} & \mathbf{O_4 - O_1 U_2^{-1} U_1} \end{bmatrix} \times \begin{bmatrix} \mathbf{a^{II}} \\ \mathbf{b^{II}} \\ \mathbf{d^{II}} \end{bmatrix} = \mathbf{0} \tag{47}$$

The premise that the matrix equation has a nonzero solution is

$$\det \begin{bmatrix} \mathbf{L_2} & \mathbf{L_3 - L_1 K_1^{-1} K_2} & \mathbf{L_4} \\ \mathbf{J_2 - J_1 H_1^{-1} H_2} & \mathbf{J_3} & \mathbf{J_4} \\ \mathbf{O_2} & \mathbf{O_3} & \mathbf{O_4 - O_1 U_2^{-1} U_1} \end{bmatrix} = \mathbf{0} \tag{48}$$

By solving matrix equation (48), one can get the value of cutoff wavenumber k_c. The value of k_c can be iteratively solved through a binary searching algorithm. When the matrix determinant is 0, the minimum value of k_c is the cut-off wavenumber of the dominant mode, and the second smallest value is the cut-off wavenumber of the first higher order mode.

III. VALIDATION AND NUMERICAL RESULTS

In order to verify the proposed method, the cutoff wavenumbers of TE waves of a T-waveguide with $a = 3.2$ mm, $b = 10.2$ mm, $c = 6.2$ mm, and $d = 8.2$ mm are computed firstly by the CST Microwave Studio. Because grid size will affect the calculation accuracy, cutoff wavenumbers are computed by CST Microwave Studio with different mesh densities. The results are shown in Table 1, where k_{c1} and k_{c2}

TABLE 1. Results of CST Microwave Studio with different mesh densities.

Cells per wavelength	k_{c1} (rad/m)	k_{c2} (rad/m)
15	166.00	392.28
30	166.21	392.70
60	166.31	393.12

TABLE 2. Results computed by the proposed method.

N	M	k_{c1} (rad/m)	k_{c2} (rad/m)
0	0	157.12	373.97
1	0	164.22	383.12
1	1	164.22	392.26
2	1	165.31	392.52
2	2	165.47	392.52
3	2	165.85	392.66
3	3	165.85	393.02

TABLE 3. Relative error of k_{c1} and k_{c2}.

N	M	Relative error	
		k_{c1} (rad/m)	k_{c2} (rad/m)
0	0	-5.53%	-4.87%
1	0	-1.26%	-2.54%
1	1	-1.26%	-0.22%
2	1	-0.60%	-0.15%
2	2	-0.51%	-0.15%
3	2	-0.28%	-0.12%
3	3	-0.28%	-0.03%

are the cutoff wavenumbers of fundamental mode and the first higher mode, respectively, and the wavelength corresponds to 20 GHz, which is slightly higher than the cutoff frequency of the first higher-order mode of the waveguide. In Table 1, it can be seen that with the increase of mesh density, the calculation results will increase slightly. Because higher mesh density results in better accuracy, the results with mesh density of sixty cells per wavelength are chosen as the baseline of comparison to study the convergence of the proposed modal expansion method.

Then, the cutoff wavenumbers are computed by the proposed method with different number of modes and the results are shown in Table 2. As shown in Table 2, the proposed method yields better agreement with the results of CST Microwave Studio as N and M increases. This is reasonable because calculation accuracy will be improved when more modes are used.

In order to evaluate the accuracy of the proposed method, it is compared with CST Microwave Studio. Table 3 shows the relative error of the two modes. From Table 3, it can be seen that the relative error drops as N and M increases, and the relative error is less than 1% when $N = 2$ and $M = 1$. Therefore, all following simulations are performed with $N = 2$ and $M = 1$. It is worth mentioning that the cutoff wavenumber of the fundamental mode requires more modes to achieve an error less than 1%. This is because the dominant field component of the fundamental mode has higher singularity than that of the first higher-order mode at the convex corners. Figs. 2 and 3 show the field pattern of the fundamental and the first higher-order modes, respectively, and the convex corners are denoted by p and q. From Fig. 2, it can be observed that E_x, the dominant field component
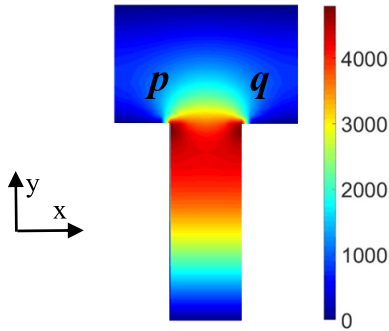
FIGURE 2. Distribution of the dominant field component (E_x) of the fundamental mode.
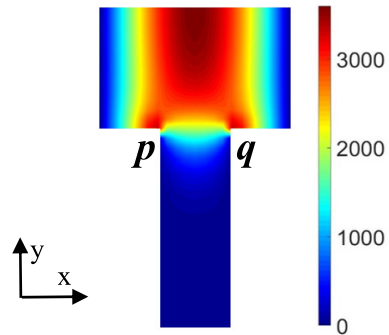

FIGURE 3. Distribution of the dominant field component (E_y) of the first higher-order mode.

of the fundamental mode, distributes over the entire region of the T-waveguide, and it reaches maximum at the convex corners p and q. On the other hand, Fig. 3 shows that E_y, the dominant field component of the first higher order mode, concentrates in the upper region of the T-waveguide. Hence, the dominant field component of the fundamental mode has higher singularity at the convex corners, and more modes are needed to accurately express the field of the fundamental mode.

It should be noted that the key interest of T-waveguide analysis is its single mode propagation characteristics, which are determined by the first two modes of the waveguide. Therefore, only the results of the first two modes are presented in Table 2. However, the proposed modal expansion method can also be used to analyze higher order modes of T-waveguide.

Fig. 4 presents the attenuation and propagation constants of the fundamental mode for this structure. The blue curve shows the result calculated by the proposed method. The red curve shows the result calculated by CST Microwave Studio. It can be observed from the figure that the two curves almost coincide. The cutoff frequency of the dominant mode in this size of T-waveguide is the point corresponding to abscissa when the ordinate is zero.

The cutoff wavenumber of the fundamental mode is one of the important parameters of waveguide design. To further characterize the cutoff wavenumber of the T-waveguide, the size of the cross section is parameterized, which is helpful for the design of the T-waveguide. Figs. 5 to 8 show the variation of cutoff wavenumber of dominant mode against
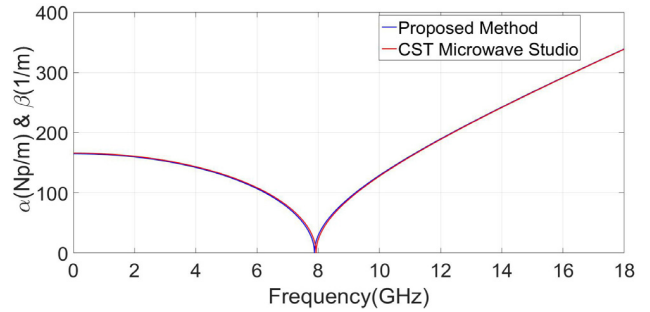

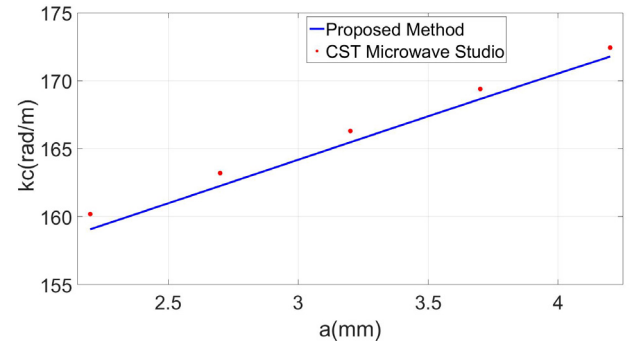**FIGURE 4.** Propagation and attenuation constant for the T-waveguide.

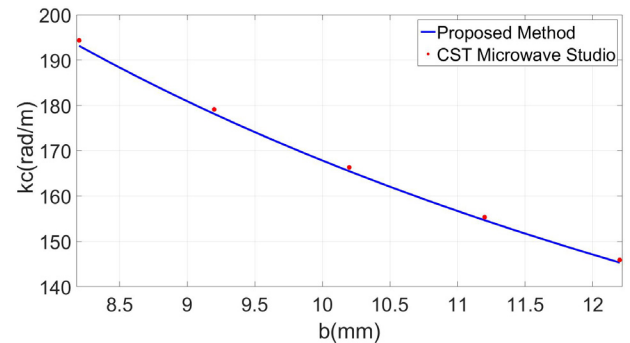**FIGURE 5.** Variation of the cut-off wavenumber versus *a*.

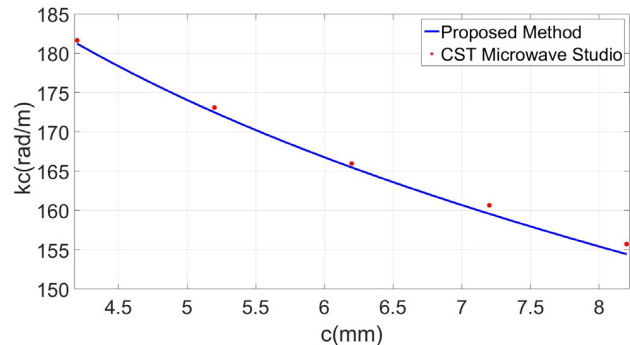**FIGURE 6.** Variation of the cut-off wavenumber versus *b*.

FIGURE 7. Variation of the cut-off wavenumber versus *c*.

the size of T-waveguide. Results obtained by the proposed method are again compared with those from CST Microwave Studio. Good agreement can be observed.

As one of the commonly used methods of waveguide analysis, modal expansion method is advantageous in terms of time and memory cost. In order to illustrate the advantage
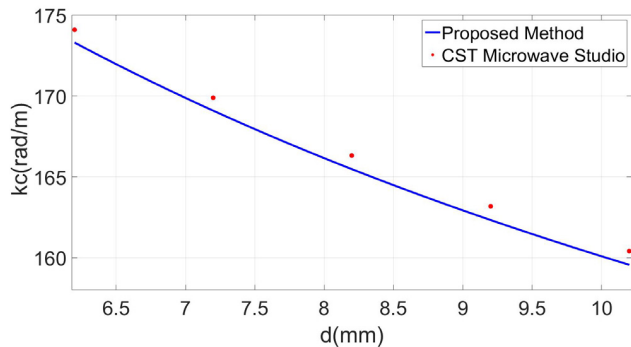
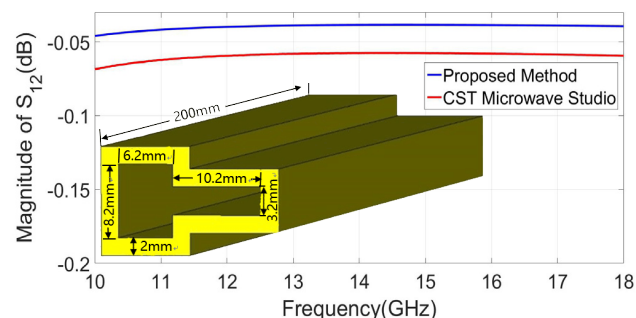**FIGURE 8.** Variation of the cut-off wavenumber versus *d*.

FIGURE 9. Transmission coefficient of the T-waveguide.

TABLE 4. Computing time and memory cost of transmission coefficient for the proposed method and cst microwave studio.

Cost comparison	CST Microwave Studio	Proposed Method
Time	40 S	1.70 S
Memory	604 MB	95 MB

Therefore, the proposed method is useful for the design of T-waveguide.

IV. CONCLUSION

The modal expansion method has been successfully applied to the calculation of T-waveguide cutoff wavenumbers. It has been demonstrated that the results obtained by the modal expansion method agree well with those obtained by CST Microwave Studio simulation. The modal expansion method needs negligible computational cost and it provides a fast and convenient way to analyze and design T-waveguide.

of the proposed method in computing time and memory, transmission coefficient of T-waveguide with a finite metallization thickness in single mode operating bandwidth is computed. The metallic material of waveguide is copper, and the electric conductivity is 5.96×10^7 S/m. The thickness, length and cross sectional dimensions of the waveguide are shown in Fig. 9. The magnitude of S_{12} is defined by

$$|S_{12}| = e^{-2\alpha z} \tag{49}$$

where α is the attenuation per unit length, and z is the length of waveguide. The attenuation per unit length is defined by

$$\alpha = \frac{P_l}{2P_t} \tag{50}$$

where

$$P_l = \frac{1}{2} R_s \int_S |J|^2 dS \tag{51}$$

is the surface conducting loss with surface resistance R_s per unit length, and

$$P_t = \frac{1}{2} Re \int_S \vec{E} \times \vec{H}^* \cdot d\vec{S} \tag{52}$$

is the average power transmitted through the waveguide. As shown in Fig. 9, results of the proposed method are close to those of CST Microwave Studio.

Table 4 shows the computing time and memory cost of transmission coefficient calculation by using the proposed method and CST Microwave Studio. According to Table 4, the proposed method is advantageous over CST Microwave Studio in terms of computational time and memory cost.

REFERENCES

[1] D. M. Pozar, *Microwave Engineering*. New York, NY, USA: Wiley, 2009.
[2] L. Guo, J. Li, W. Huang, H. Shao, T. Ba, T. Jiang, Y. Jiang, Y. Jiang, and G. Deng, "A waveguide magic-T with coplanar arms for high-power solid-state power combining," *IEEE Trans. Microw. Theory Techn.*, vol. 65, no. 8, pp. 2942–2952, Aug. 2017.
[3] M. Amjadi and E. Jafari, "Design of a broadband eight-way coaxial waveguide power combiner," *IEEE Trans. Microw. Theory Techn.*, vol. 60, no. 1, pp. 39–45, Jan. 2012.
[4] B. Zhang, K. Song, X. Wang, Y. Yan, Y. Zhou, and Y. Fan, "Compact quasi-planar four-way power divider with wide isolation bandwidth," *IEEE Access*, vol. 7, pp. 77915–77922, May 2019.
[5] D. Wu, F. Liu, X. Wang, H. Xu, L. Zhang, W. Xu, Y. Tang, and J. Wang, "The design of directional coupler for ECRH system," *IEEE Access*, vol. 5, pp. 6187–6191, Apr. 2017.
[6] T. R. Jones and M. Daneshmand, "Miniaturized slotted bandpass filter design using a ridged half-mode substrate integrated waveguide," *IEEE Microw. Wireless Compon. Lett.*, vol. 26, no. 5, pp. 334–336, May 2016.
[7] Y. D. Dong, T. Yang, and T. Itoh, "Substrate integrated waveguide loaded by complementary split-ring resonators and its applications to miniaturized waveguide filters," *IEEE Trans. Microw. Theory Techn.*, vol. 57, no. 9, pp. 2211–2223, Sep. 2009.
[8] Z. Liu, J.-Y. Deng, and D. Sun, "Slow-wave groove gap waveguide bandpass filter," *IEEE Access*, vol. 7, pp. 52581–52588, Apr. 2019.
[9] L. W. Epp, D. J. Hoppe, A. R. Khan, and S. L. Stride, "A high-power *Ka*-band (31–36 GHz) solid-state amplifier based on low-loss corporate waveguide combining," *IEEE Trans. Microw. Theory Techn.*, vol. 56, no. 8, pp. 1899–1908, Aug. 2008.
[10] Y. Yi, H. Wang, Y. Liu, M. Jiang, X. Wang, F. Wang, and D. Zhang, "Multilayer hybrid waveguide amplifier for three-dimension photonic integrated circuit," *IEEE Photon. Technol. Lett.*, vol. 27, no. 22, pp. 2411–2413, Nov. 15, 2015.
[11] S.-J. Park, D.-H. Shin, and S.-O. Park, "Low side-lobe substrate-integrated-waveguide antenna array using broadband unequal feeding network for millimeter-wave handset device," *IEEE Trans. Antennas Propag.*, vol. 64, no. 3, pp. 923–932, Mar. 2016.
[12] K. Gong, Z. N. Chen, X. Qing, P. Chen, and W. Hong, "Substrate integrated waveguide cavity-backed wide slot antenna for 60-GHz bands," *IEEE Trans. Antennas Propag.*, vol. 60, no. 12, pp. 6023–6026, Dec. 2012.
[13] G. P. Le Sage, "3D printed waveguide slot array antennas," *IEEE Access*, vol. 4, pp. 1258–1265, 2016.
[14] A. Beltayib, I. Afifi, and A.-R. Sebak, "4 × 4-element cavity slot antenna differentially-fed by odd mode ridge gap waveguide," *IEEE Access.*, vol. 7, pp. 48185–48195, Apr. 2019.
[15] A. Berenguer, V. Fusco, D. E. Zelenchuk, D. Sánchez-Escuderos, M. Baquero-Escudero, and V. E. Boria-Esbert, "Propagation characteristics of groove gap waveguide below and above cutoff," *IEEE Trans. Microw. Theory Techn.*, vol. 64, no. 1, pp. 27–36, Jan. 2016.

[16] T. V. Smitha and K. V. Nagaraja, "Application of automated cubic-order mesh generation for efficient energy transfer using parabolic arcs for microwave problems," *Energy*, vol. 168, pp. 1104–1118, Feb. 2019.

[17] X. Kuang, Z. Huang, M. Chen, and X. Wu, "High-order symplectic compact finite-different time-domain algorithm for guide-wave structures," *IEEE Microw. Wireless Compon. Lett.*, vol. 29, no. 2, pp. 80–82, Feb. 2019.

[18] H. Zhao and Z. Shen, "Modal-expansion analysis of a monopole in vibrating reverberation chamber," *Prog. Electromagn. Res.*, vol. 85, pp. 303–322, 2008.

[19] A. Luciano, B. Giorgio, and M. Mauro, "Modal loss analysis of *E*- and *H*-plane filtering structures," *IEEE Trans. Microw. Theory Techn.*, vol. 63, no. 1, pp. 40–47, Jan. 2015.

[20] L. Kuhler, G. Le Fur, L. Duchesne, and N. Raveu, "The propagation characteristics of 2-D metamaterial waveguides using the modal expansion theory," *IEEE Trans. Microw. Theory Techn.*, vol. 66, no. 10, pp. 4319–4326, Oct. 2018.

[21] J. H. Kim and H. J. Eom, "Radiation from multiple annular slots on a circular cylindrical cavity," *J. Electromagn. Waves Appl.*, vol. 21, no. 1, pp. 47–56, Jan. 2007.

[22] J. Ock and H. Eom, "Radiation of a hertzian dipole in a shortended conducting circular cylinder with narrow circumferential slots," *Prog. Electromagn. Res. Lett.*, vol. 2, pp. 11–20, 2008.

[23] Y. Utsumi, "Variational analysis of ridged waveguide modes," *IEEE Trans. Microw. Theory Techn.*, vol. MTT-33, no. 2, pp. 111–120, Feb. 1985.

KANGNING LI (S'18) was born in Baoding, Hebei, China, in 1994. She received the bachelor's degree in communication engineering from Hebei Technological University, Tianjin, China, in July 2017. She is currently pursuing the master's degree with the School of Electronic Science and Engineering, University of Electronic Science and Technology of China, Chengdu, China. Her research interests include the electromagnetic analysis and design of passive microwave components and high speed interconnects.

HUAPENG ZHAO (S'08–M'12) was born in Hebei, China, in 1983. He received the bachelor's and master's degrees in electromagnetic field and microwave technology from the University of Electronic Science and Technology of China, Chengdu, China, in July 2004 and March 2007, respectively, and the Ph.D. degree in communication engineering from Nanyang Technological University, Singapore, in June 2012. He was a Scientist with the Institute of High Performance Computing, Agency for Science, Technology and Research (A∗STAR), Singapore, from August 2011 to December 2015. Since December 2015, he has been an Associate Professor with the School of Electronic Science and Engineering, University of Electronic Science and Technology of China, Chengdu. He has authored or coauthored more than 100 technical articles published in international journals or conferences. His current research interests include system-level electromagnetic analysis and design, and signal and data processing techniques in electromagnetics.

Dr. Zhao is a member of the Organizing Committee/Technical Program Committee of several international conferences. He was a recipient of the 2016 IEEE Asia–Pacific Electromagnetic Compatibility Young Scientist Award and the 2014 URSI Young Scientist Award. He was the Technical Program Chair of the 2016 Asia Wireless Power Transfer Workshop. He was a Guest Editor of the *International Journal of Antennas and Propagation* and currently serves the Associate Editor of IEEE ACCESS.

MINGZHOU ZHAN (M'10) received the B.Sc. (Eng.), M.Sc. (Eng.), and Ph.D. degrees from the University of Electronic Science and Technology of China (UETSC), Chengdu, China, in 2004, 2007, and 2010, respectively, all in electromagnetic field and microwave technology, where he was a Research Assistant with the Laboratory of Microwave and Millimeter-Wave MCM Technology and also with the Key Laboratory of Very High Frequency Complex Systems, from 2007 to 2010 and he is currently an Associate Professor with the School of Electronic Science and Engineering. His current research interest includes millimeter-wave integrated circuits and systems.

· · ·